

Striking light-induced nonadiabatic fingerprint in the low-energy vibronic spectra of polyatomic molecules

Csaba Fábri^{1,2}, Benjamin Lasorne³, Gábor J. Halász⁴, Lorenz S. Cederbaum⁵, and Ágnes Vibók^{6,7}

¹Laboratory of Molecular Structure and Dynamics, Institute of Chemistry, Eötvös Loránd University, Pázmány Péter sétány 1/A, H-1117 Budapest, Hungary; E-mail: ficsaba@caesar.elte.hu

²MTA-ELTE Complex Chemical Systems Research Group, P.O. Box 32, H-1518 Budapest 112, Hungary

³Institut Charles Gerhardt Montpellier (ICGM), Université de Montpellier, CNRS, ENSCM, F-34095 Montpellier, France

⁴Department of Information Technology, University of Debrecen, P.O. Box 400, H-4002 Debrecen, Hungary

⁵Theoretische Chemie, Physikalisch-Chemisches Institut, Universität Heidelberg, Im Neuenheimer Feld 229, 69120 Heidelberg, Germany

⁶Department of Theoretical Physics, University of Debrecen, PO Box 400, H-4002 Debrecen, Hungary; E-mail: vibok@phys.unideb.hu

⁷ELI-ALPS, ELI-HU Non-Profit Ltd, H-6720 Szeged, Dugonics tér 13, Hungary

January 24, 2022

Abstract

Nonadiabaticity, i.e., the effect of mixing electronic states by nuclear motion, is a central phenomenon in molecular science. The strongest nonadiabatic effects arise due to the presence of conical intersections of electronic energy surfaces. These intersections are abundant in polyatomic molecules. Laser light can induce in a controlled manner new conical intersections, called light-induced conical intersections, which lead to strong nonadiabatic effects similar to those of the natural conical intersections. These effects are, however, controllable and may even compete with those of the natural intersections. In this work we show that the standard low-energy vibrational spectrum of the electronic ground state can change dramatically by inducing nonadiabaticity via a light-induced conical intersection. This generic effect is demonstrated for an explicit example by full-dimensional high-level quantum calculations using a pump-probe scheme with a moderate-intensity pump laser and a weak probe laser.

1 Introduction

Nonadiabatic phenomena^{1–6} occurring in polyatomic molecules have been known for decades to play a fundamental role in most photobiological, photochemical, and photophysical processes.^{7–18} Such effects become significant around molecular geometries where two (or more) potential energy surfaces (PESs) are energetically degenerate, such that the Born–Oppenheimer (BO) approximation¹⁹ breaks down. This yields strong mixing among BO electronic states and subsequent radiationless transitions correlated with variations of the molecular geometry (nuclear degrees of freedom).

Such degeneracy points, termed conical intersections (CIs), are characterized locally by a two-dimensional subspace within the space spanned by the nuclear degrees of freedom, the so-called “branching” space (BS) along which the degeneracy is lifted to first order around the CI. This can occur only in molecules with more than two atoms (Wigner’s noncrossing rule).²⁰ Indeed, diatomic molecules have a single vibrational coordinate, which cannot accommodate both zero energy-difference tuning and zero coupling except for symmetry reasons. CIs provide ultrafast nonradiative decay channels for electronically excited molecules. In the vicinity of such points, nonadiabatic dynamics (beyond BO) takes place typically on the femtosecond time scale (~ 10 – 100 fs). While it is by now well established that they are present in small- or medium-sized molecules, CIs have been shown to be ubiquitous in large molecular systems, hence playing a key role in most photoinduced processes.

More than a decade ago, it has been demonstrated that laser light with significant intensity (dressed-state regime) can in turn induce CI-type situations between field-dressed PESs and thus give rise to new types of nonadiabatic phenomena, even in diatomic molecules.^{21,22} Such points were then termed light-induced conical intersections (LICIs). Whereas the location of a “natural” CI in a field-free polyatomic molecule and the strength of the nonadiabatic coupling are inherent properties of the system, the occurrence of the crossing point is determined by the laser frequency while the strength of the nonadiabatic-type coupling is controlled by the laser intensity.

Several theoretical and experimental works have demonstrated on both fronts that LICIs give rise to a variety of unexpected nonadiabatic phenomena in molecules,^{23–27} with significant impact on various dynamical^{28–31} and spectroscopic properties.^{32–35} These works were mainly focused on diatomic molecules where the angle between the internuclear axis and the field polarization axis provides the missing degree of freedom for a CI to emerge between two crossing field-dressed PESs. This rotation angle together with the internuclear separation span the two-dimensional light-induced BS along which degeneracy is lifted to first order around the LICI due to the dressing field.

Investigating light-induced nonadiabatic effects in polyatomic molecules is expected to be more challenging than in diatomics. On the one hand, the existence of several vibrational degrees of freedom enables a two-dimensional BS to be defined without further involving any rotational coordinate. On the other hand, natural CIs are so ubiquitous in polyatomics that their occurrence, with subsequent natural nonadiabatic effects, are likely to be strongly mixed with the light-induced ones. It is thus desirable to consider situations where a clear separation

and identification of the effects of natural and light-induced conical intersections can be made, so as to clarify and understand the effect solely caused by the LICI.

Experimental works^{36,37} have already invoked the concept of a LICI to provide qualitative interpretation to the results of laser-induced isomerization and photodissociation in polyatomic molecules. A general theory on LICIs in polyatomics discusses strategies of its exploitation and application in such systems.³⁸ The present study goes beyond previous investigations and makes an attempt to identify some “direct observable signature” of LICIs in polyatomic molecules.

It is well established in the field of “natural” nonadiabatic molecular phenomena that the breakdown of the BO approximation induces strong mixing between the vibrational levels within coupled adiabatic PESs. The Franck–Condon approximation is no longer valid, which typically leads at low energies to the so-called “intensity borrowing” effect.¹ This is a characteristic fingerprint of nonadiabatic effects in molecular spectroscopy, manifested by irregular variations of spectral peak intensities and the appearance of unexpected levels.

Along this line, our current work presents strong intensity-borrowing effects, now appearing in the field-dressed low-energy vibronic spectrum of the H₂CO (formaldehyde) molecule and absent in the absence of the field, providing direct evidence for the LICI and its effect. The photochemistry of H₂CO has been studied in various contexts and the corresponding literature is abundant and beyond the scope of the present work. We chose H₂CO for two reasons: first, because there is no natural CI in the vicinity of the Franck–Condon region. A seam of CIs has been characterized for example by Araujo et al.^{39–41} but it is protected by a transition barrier at low energies; second, this system presents the great advantage of not having any first-order nonadiabatic coupling between the ground and first singlet excited electronic states around its equilibrium geometry. As a consequence, such a situation allows unambiguous identification of light-induced nonadiabatic phenomena, clearly separated from other “natural” nonadiabatic effects.

By using a two-step protocol we simulate the weak-field absorption and stimulated emission spectra of the *field-dressed* H₂CO molecule at low energy (infrared domain) taking into account all six vibrational degrees of freedom explicitly. First, we compute the field-dressed states which are superpositions of field-free molecular eigenstates coupled by a medium-intensity laser dressing pump pulse switched on adiabatically. Second, we assume that the low-energy spectrum of the field-dressed molecule can be accessed with a weak-intensity steady-state probe. The dipole transition amplitudes between the field-dressed states are thus evaluated within the typical framework of first-order time-dependent perturbation theory, revealing intensity borrowing in the infrared domain for the field-dressed molecule.

2 Theory and computational protocol

2.1 Working Hamiltonian

Let us start with describing the working Hamiltonian and the protocol used to compute field-dressed states and field-dressed spectra. Throughout the current work the two singlet electronic states S₀ (\tilde{X}^1A_1) and S₁ (\tilde{A}^1A_2) of H₂CO are taken into account, the corresponding six-dimensional PESs are denoted by V_X and V_A , respectively. We assume that the electronic states X and A are coupled by a time-dependent external electric field $\mathbf{E}(t) = \mathbf{E}_0 \cos(\omega t)$. In the static Floquet-state representation^{42,43} the Hamiltonian matrix has the following form

$$\hat{H} = \begin{bmatrix} \hat{T} & 0 \\ 0 & \hat{T} \end{bmatrix} + \begin{bmatrix} V_X + n\hbar\omega & W \\ W & V_A + (n-1)\hbar\omega \end{bmatrix} \quad (1)$$

where \hat{T} is the vibrational kinetic energy operator constructed in a fully exact and numerical way^{44,45} and n is the Fourier index that labels the different light-induced potential channels. The operator $W = -\mathbf{d}(\mathbf{R})\mathbf{e}E_0/2$ describes the coupling between the electronic states X and A with $\mathbf{d}(\mathbf{R})$ being the body-fixed molecular transition dipole moment (TDM) vector depending on the vibrational coordinates \mathbf{R} . Moreover, \mathbf{e} , E_0 and ω denote the polarization,

amplitude and angular frequency of the dressing laser field, respectively. We used linearly-polarized electric fields throughout this work. The rotational degrees of freedom were omitted from our computational protocol and the orientation of the molecule was fixed with respect to the external electric field. Finally, we note that in all practical computations we went beyond the approximate two-by-two Floquet Hamiltonian of eqn (1) and used the following light-dressed Hamiltonian

$$\hat{H} = \begin{bmatrix} \hat{H}_{-n_{\max}} & \hat{D} & 0 & 0 & 0 & 0 & 0 \\ \hat{D}^\dagger & \ddots & \vdots & \vdots & \vdots & \ddots & 0 \\ 0 & \cdots & \hat{H}_{-1} & \hat{D} & 0 & \cdots & 0 \\ 0 & \cdots & \hat{D}^\dagger & \hat{H}_0 & \hat{D} & \cdots & 0 \\ 0 & \cdots & 0 & \hat{D}^\dagger & \hat{H}_1 & \cdots & 0 \\ 0 & \ddots & \vdots & \vdots & \vdots & \ddots & \hat{D} \\ 0 & 0 & 0 & 0 & 0 & \hat{D}^\dagger & \hat{H}_{n_{\max}} \end{bmatrix} \quad (2)$$

with

$$\hat{H}_n = \begin{bmatrix} \hat{T} + V_X + n\hbar\omega & 0 \\ 0 & \hat{T} + V_A + n\hbar\omega \end{bmatrix} \quad (3)$$

and

$$\hat{D} = \begin{bmatrix} W_X & W \\ W & W_A \end{bmatrix} \quad (4)$$

where the terms $W_X = -\mathbf{d}_X(\mathbf{R})\mathbf{e}E_0/2$ and $W_A = -\mathbf{d}_A(\mathbf{R})\mathbf{e}E_0/2$ describe the interaction between the external electric field and the permanent dipole moments (PDMs) of the electronic states X and A.⁴⁶ In what follows, for the sake of simplicity, the discussion will be limited to the two-by-two Floquet Hamiltonian of eqn (1).

After diagonalizing the potential energy matrix of eqn (1) one can obtain the adiabatic potential energy surfaces V_{lower} and V_{upper} . These two PESs can cross each other, giving rise to a LICI, whenever the conditions $W = 0$ and $V_X = V_A - \hbar\omega$ are simultaneously fulfilled.

The field-dressed eigenfunctions $|\Phi_k(n)\rangle$ and quasienergies $\varepsilon_k(n)$ can be obtained by determining the eigenpairs of the Hamiltonian of eqn (1). The eigenfunctions $|\Phi_k(n)\rangle$ can be expanded as the linear combination of products of field-free molecular vibronic eigenstates (denoted by $|Xi\rangle$ and $|Ai\rangle$ for the electronic states X and A, respectively) and the Fourier vectors of the Floquet states, that is

$$|\Phi_k(n)\rangle = \sum_i C_{Xi}^{(k)} |Xi\rangle |n\rangle + \sum_i C_{Ai}^{(k)} |Ai\rangle |n-1\rangle. \quad (5)$$

In eqn (5) i labels vibrational eigenstates and $|n\rangle$ is the n th Fourier vector of the Floquet state. The expansion coefficients $C_{Xi}^{(k)}$ and $C_{Ai}^{(k)}$ can be obtained by diagonalizing the light-dressed Hamiltonian of eqn (1) after constructing its matrix representation.

To move forward, we briefly discuss the spectroscopy of field-dressed molecules.³⁴ Namely, we compute transition amplitudes between field-dressed states $|\Phi_k(n)\rangle$ and $|\Phi_l(m)\rangle$ assuming a weak probe pulse which allows us to use first-order time-dependent perturbation theory for the evaluation of transition amplitudes following the standard procedure of theoretical molecular spectroscopy.⁴⁷ The transition amplitudes are the matrix elements of the electric dipole moment operator \hat{d}_α ($\alpha = x, y, z$) between two field-dressed states of eqn (5),

$$\begin{aligned} \langle \Phi_k(n) | \hat{d}_\alpha | \Phi_l(m) \rangle = \\ \sum_i \sum_j C_{Xi}^{(k)*} C_{Xj}^{(l)} \langle Xi | \hat{d}_\alpha | Xj \rangle + \sum_i \sum_j C_{Ai}^{(k)*} C_{Aj}^{(l)} \langle Ai | \hat{d}_\alpha | Aj \rangle \end{aligned} \quad (6)$$

and

$$\begin{aligned}
\langle \Phi_k(n) | \hat{d}_\alpha | \Phi_l(m) \rangle = & \\
\delta_{m,n+1} \sum_i \sum_j C_{Xi}^{(k)*} C_{Aj}^{(l)} \langle Xi | \hat{d}_\alpha | Aj \rangle + & \\
\delta_{m,n-1} \sum_i \sum_j C_{Ai}^{(k)*} C_{Xj}^{(l)} \langle Ai | \hat{d}_\alpha | Xj \rangle &
\end{aligned} \tag{7}$$

where $n \neq m$. One can notice that while transitions $|\Phi_k(n)\rangle \rightarrow |\Phi_l(n)\rangle$ are associated with the PDMs related to the electronic states X and A, the transitions $|\Phi_k(n)\rangle \rightarrow |\Phi_l(n+1)\rangle$ and $|\Phi_k(n)\rangle \rightarrow |\Phi_l(n-1)\rangle$ are governed by the TDM. The corresponding transition energies are $\epsilon_l(n) - \epsilon_k(n)$, $\epsilon_l(n+1) - \epsilon_k(n) = \epsilon_l(n) - \epsilon_k(n) + \hbar\omega$ and $\epsilon_l(n-1) - \epsilon_k(n) = \epsilon_l(n) - \epsilon_k(n) - \hbar\omega$, respectively. Eqn (6) serves as our working formula for the computation of the low-energy part of the vibronic spectrum. The expressions of eqn (6) and eqn (7) pertain to both the field-dressed absorption and stimulated emission processes. Peaks associated with absorption and stimulated emission are separated by comparing the quasienergies of the initial and final field-dressed states. The intensity of transitions between field-dressed states can be obtained as

$$I_{kl} \propto \omega_{kl} \sum_{\alpha=x,y,z} |\langle \Phi_k(n) | \hat{d}_\alpha | \Phi_l(m) \rangle|^2 \tag{8}$$

where ω_{kl} denotes the transition frequency.

2.2 The H₂CO molecule and technical details

The V_X (S_0 electronic state, X) and V_A (S_1 electronic state, A) PESs were taken from refs. 48 and 49, respectively, the corresponding vertical and adiabatic excitation energies are 28954 cm⁻¹ and 28138 cm⁻¹. The planar ground-state (X) equilibrium structure of H₂CO (C_{2v} point-group symmetry) is shown in Fig. 1 while its normal modes are summarized in Fig. 2 and Table 1. Note that the definition of the Cartesian axes in Fig. 1 is in line with the Mulliken convention.⁵⁰ The excited electronic state (A) has a double-well structure along the out-of-plane (v_4) mode and the two equivalent nonplanar equilibrium structures are connected by a planar transition state structure, the respective barrier height is 315 cm⁻¹.

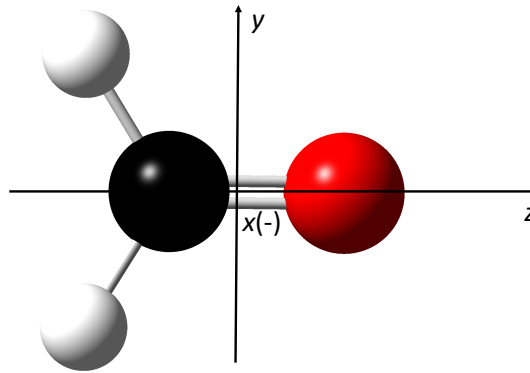


Figure 1: Equilibrium structure of the H₂CO molecule in its electronic ground state (X) and the body-fixed coordinate system chosen (the x axis is directed inwards, as indicated by the - sign).

The six-dimensional vibrational Schrödinger equation was solved variationally by the numerically exact and general rovibrational code GENIUSH^{44,45,51} for both PESs. The body-fixed Cartesian position vectors of the nuclei

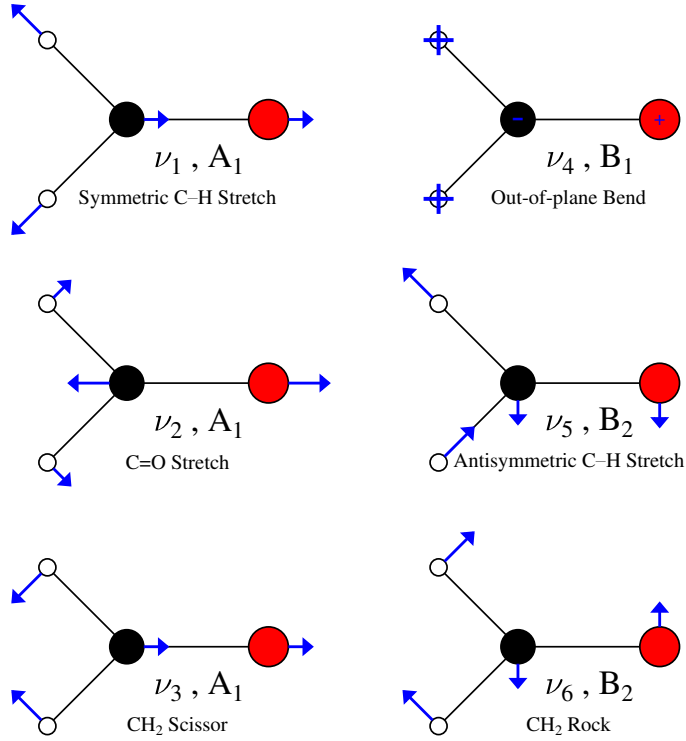


Figure 2: Normal modes of the H_2CO molecule.

Table 1: Normal mode labels, C_{2v} irreducible representations, description of normal modes and anharmonic fundamentals (obtained by 6D variational computations in the electronic ground state (X) of H_2CO , in units of cm^{-1}).

mode	symmetry	description	ω/cm^{-1}
ν_1	A_1	sym C-H stretch	2728.4
ν_2	A_1	C=O stretch	1738.1
ν_3	A_1	CH_2 scissor	1466.0
ν_4	B_1	out-of-plane bend	1147.0
ν_5	B_2	antisym C-H stretch	2819.9
ν_6	B_2	CH_2 rock	1234.5

were parameterized using polyspherical coordinates⁵² and the body-fixed axes were oriented according to Eckart conditions⁵³ using the equilibrium structure of the X electronic state as reference structure. A symmetry-adapted six-dimensional direct-product discrete variable representation (DVR) basis and atomic mass values $m_{\text{C}} = 12.0\text{u}$, $m_{\text{O}} = 15.994915\text{u}$ and $m_{\text{H}} = 1.007825\text{u}$ were employed throughout the nuclear motion computations. The vibrational Hamiltonian matrix was separated into four blocks corresponding to the four irreducible representations of the S_2^* molecular symmetry group⁴⁷ which is isomorphic to the C_{2v} point group. In order to assist the interpretation of the field-dressed spectra presented in Section 3, the vibrational eigenstates of the A electronic state were recomputed using the DEWE program package^{54,55} and the rectilinear normal coordinates corresponding to the planar transition state structure of the A electronic state. Then, one-dimensional wave function cuts along the normal coordinates were evaluated and the nodal structure of these one-dimensional cuts was inspected to assign the eigenstates with vibrational quantum numbers.

The permanent and transition dipole moment, i.e., PDM and TDM, surfaces required by the computation of the

field-dressed states and transition amplitudes, were generated by Taylor expansions up to second order using the polyspherical coordinates employed by the vibrational eigenstate computations. The Taylor series are centered at the equilibrium structure of the X electronic state (TDM and X-state PDM) and at the transition state structure of the A electronic state (A-state PDM), respectively. The PDM and TDM components were referenced in the Eckart frame described above and the necessary dipole derivatives were evaluated numerically at the CAM-B3LYP/6-31G* level of theory. The symmetry properties of the body-fixed PDM and TDM components are summarized in Table 2. The field-dressed states were computed by diagonalizing the light-dressed Hamiltonian of eqn (2) in the direct-product basis of field-free molecular eigenstates and Fourier vectors of the Floquet states $|n\rangle$, the maximal Fourier component was set to $n_{\max} = 2$ which was sufficient for obtaining converged results.

Table 2: Symmetry properties (C_{2v} irreducible representations) of the body-fixed components of the permanent (PDM) and transition (TDM) dipole moments.

	PDM	TDM
x	B_1	B_2
y	B_2	B_1
z	A_1	A_2

The symmetries of the X and A electronic states are A_1 and A_2 at the Franck–Condon point of C_{2v} symmetry. According to Table 1, H_2CO does not have any vibrational modes of A_2 symmetry, and therefore, there is no vibration available for the expansion of the first-order nonadiabatic coupling of A_2 symmetry at the Franck–Condon point. In addition, all components of the TDM vanish at the Franck–Condon point due to symmetry and hence all natural and light-induced couplings are zero at C_{2v} geometries. The x -component of the TDM is a linear function of both B_2 modes, while the y -component is a linear function of the B_1 mode, which can induce LICIs when distorting the geometry for a given field polarization.

2.3 Dressing mechanism and light-induced conical intersections

In what follows, a simple model facilitating the analysis of the field-dressed spectra presented in Section 3 is outlined. We assume that the dressing field is turned on adiabatically and the initial field-dressed state $|\Phi_i(n)\rangle$ is chosen as the field-dressed state which gives maximal overlap with the vibrational ground state of the X electronic state. If the dressing field couples the vibrational ground state of X to N vibrational eigenstates of A, the initial field-dressed state becomes

$$|\Phi_i(n)\rangle = C_{X0}^{(i)}|X0\rangle|n\rangle + \sum_{k=1}^N C_{Ak}^{(i)}|Ak\rangle|n-1\rangle. \quad (9)$$

Such a situation is featured in Fig. 3 where one-dimensional cuts of the V_X and V_A PESs are shown along the v_2 normal mode (normal coordinates other than Q_2 are set to zero). In Fig. 3, the system is dressed with photons corresponding to $\omega = 32935 \text{ cm}^{-1}$ and the V_A PES is shifted down with the energy of the dressing photon. Consequently, the vibrational ground state of X becomes nearly resonant with multiple close-lying excited vibrational eigenstates of A and field-dressed states of eqn (9) are formed. Fig. 4 provides two-dimensional cuts of the resulting light-induced adiabatic PESs with the dressing wavenumber of $\omega_d = 29000 \text{ cm}^{-1}$ and dressing intensity of $I_d = 10^{14} \text{ W/cm}^2$ (the dressing field is polarized along the body-fixed y axis). The two-dimensional cuts, given as functions of the Q_2 and Q_4 normal coordinates (the remaining four normal coordinates are set to zero), clearly show that a LICI is formed between the two light-induced adiabatic PESs.

If the final field-dressed state remains an eigenstate of the field-free molecule, that is,

$$|\Phi_j(n)\rangle = |Xj\rangle|n\rangle \quad (10)$$

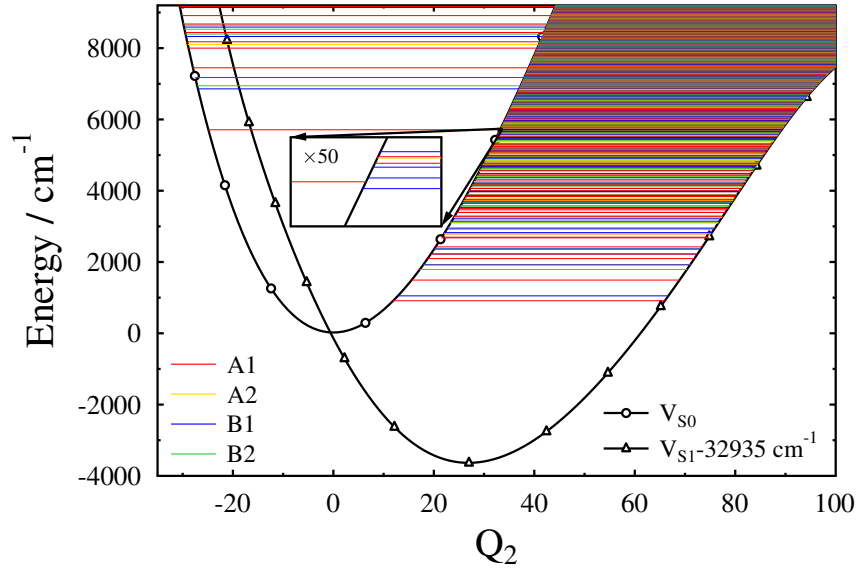


Figure 3: One-dimensional field-free potential energy cuts along the ν_2 (C=O stretch) normal mode. The excited-state potential curve (V_{S1} in the figure) is shifted down by the photon energy value corresponding to 32935 cm^{-1} . Vibrational energy levels are indicated by horizontal lines with colours encoding irreducible representations of the C_{2v} point group.

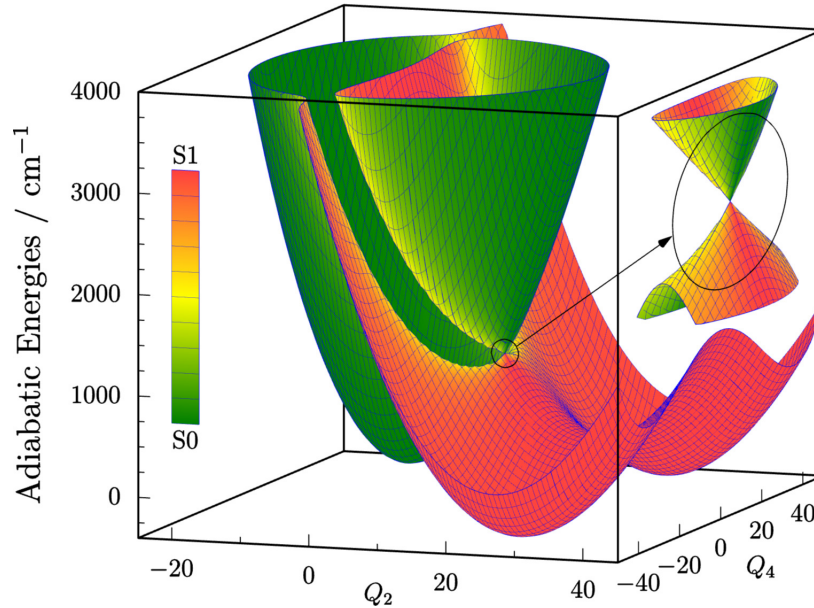


Figure 4: Two-dimensional light-induced adiabatic potential energy surfaces along the ν_2 (C=O stretch) and ν_4 (out-of-plane bend) normal modes. The dressing wavenumber and intensity are chosen as $\omega_d = 29000 \text{ cm}^{-1}$ and $I_d = 10^{14} \text{ W/cm}^2$, respectively, and the dressing field is polarized along the body-fixed y axis. This intensity is chosen for a better visualization only. The light-induced conical intersection is highlighted in the inset on the right-hand side of the figure. The character of the adiabatic potential energy surfaces is indicated by different colours (see the legend on the left).

or

$$|\Phi_{j'}(n)\rangle = |Aj'\rangle|n-1\rangle, \quad (11)$$

then the transition amplitudes for the transitions $|\Phi_i(n)\rangle \rightarrow |\Phi_j(n)\rangle$ and $|\Phi_i(n)\rangle \rightarrow |\Phi_{j'}(n)\rangle$ take the form

$$\langle\Phi_j(n)|\hat{d}_\alpha|\Phi_i(n)\rangle = C_{X0}^{(i)}\langle Xj|\hat{d}_\alpha|X0\rangle \quad (12)$$

and

$$\langle\Phi_{j'}(n)|\hat{d}_\alpha|\Phi_i(n)\rangle = \sum_{k=1}^N C_{Ak}^{(i)}\langle Aj'|\hat{d}_\alpha|Ak\rangle. \quad (13)$$

The physical interpretation of the previous equations is outlined as follows. Peaks that correspond to the transitions $|X0\rangle \rightarrow |Xj\rangle$ of the field-free vibrational spectrum appear also in the field-dressed spectrum, but their intensities in the field-dressed case are proportional to $|C_{X0}^{(i)}\langle Xj|\hat{d}_\alpha|X0\rangle|^2$ (see eqn (12)), falling short of the corresponding field-free intensity values since $|C_{X0}^{(i)}|^2 < 1$. The second group of peaks (see eqn (13)) appear only in the field-dressed case as a consequence of the field-induced couplings between the vibrational ground state of X and vibrational eigenstates of A. As we will see in Section 3, these peaks appear primarily in the lower half of the studied region of the field-dressed spectrum and they are associated with the PDM of the A electronic state according to eqn (13).

3 Results and discussion

Let us start with the field-free vibrational spectrum of H_2CO in its electronic ground state X, shown in Fig. 5. The spectrum in Fig. 5 was computed using the six-dimensional variational vibrational eigenstates provided by GENIUSH^{44,45,51} and the PDM surface of the X electronic state described in Section 2.2. The field-free vibrational spectrum has been found to agree well with the anharmonic vibrational spectrum computed by the Gaussian 09 program package.⁵⁶ As expected, the field-free vibrational spectrum consists of a moderate number of peaks, corresponding to vibrational transitions from the initially populated vibrational ground state to vibrationally-excited eigenstates. Besides the six fundamental transitions (denoted with the normal mode labels ν_i in Fig. 5) two combination transitions ($\nu_2 + \nu_6$ and $\nu_3 + \nu_6$) and an overtone transition ($2\nu_2$) carry appreciable intensity. It is clearly visible in Fig. 5 that no peaks appear below 1100 cm^{-1} in the field-free vibrational spectrum.

We now turn to the discussion of the field-dressed spectra. In the computations several values of the dressing intensity, ranging from $I_d = 10^8 \text{ W/cm}^2$ to $I_d = 10^{11} \text{ W/cm}^2$, and of the dressing wavenumber, ranging from $\omega_d = 28000 \text{ cm}^{-1}$ to $\omega_d = 35000 \text{ cm}^{-1}$ (or from $\lambda_d = 357.14 \text{ nm}$ to $\lambda_d = 285.71 \text{ nm}$ in units of wavelength), were applied. In the following we consider different dressing situations that lead to striking effects in the field-dressed spectra. Fig. 6 shows the absorption (solid line) and stimulated emission (dashed line) spectra of H_2CO molecule dressed with a laser field linearly polarized along the body-fixed y axis with $I_d = 10^{11} \text{ W/cm}^2$ and $\omega_d = 32932.5 \text{ cm}^{-1}$ ($\lambda_d = 303.65 \text{ nm}$). Two prominent features of the field-dressed spectrum in Fig. 6 are the emergence of several peaks below 1100 cm^{-1} , as opposed to the field-free vibrational spectrum, and the appearance of induced emission peaks which are completely missing from the field-free vibrational spectrum.

The newly-emerging peaks, readily visible in the lower panel of Fig. 6, can be classified into four main groups. The first two groups consist of peaks between $400 - 650 \text{ cm}^{-1}$ (g_1) and $700 - 800 \text{ cm}^{-1}$ (g_2), while the third and fourth groups involve peaks located in the intervals $800 - 900 \text{ cm}^{-1}$ (g_3) and $1000 - 1100 \text{ cm}^{-1}$ (g_4). The transitions of g_1 and g_2 types are all polarized along the body-fixed x axis, while the g_3 and g_4 transitions are polarized along the body-fixed y (hardly discernible in Fig. 6) and z axes, respectively. As already discussed in Section 2.3, the peaks appearing below 1100 cm^{-1} in the field-dressed spectrum can be attributed to admixtures of the vibrational eigenstates of the A electronic state in the initial field-dressed state of eqn (9). The initial field-dressed state in this particular case is a superposition of the X vibrational ground state (0.0 cm^{-1} , A_1 symmetry, 52.3%) and two close-lying A vibrational eigenstates of B_1 symmetry, namely 32931.2 cm^{-1} (36.0%) and 32937.2 cm^{-1} (11.5%)

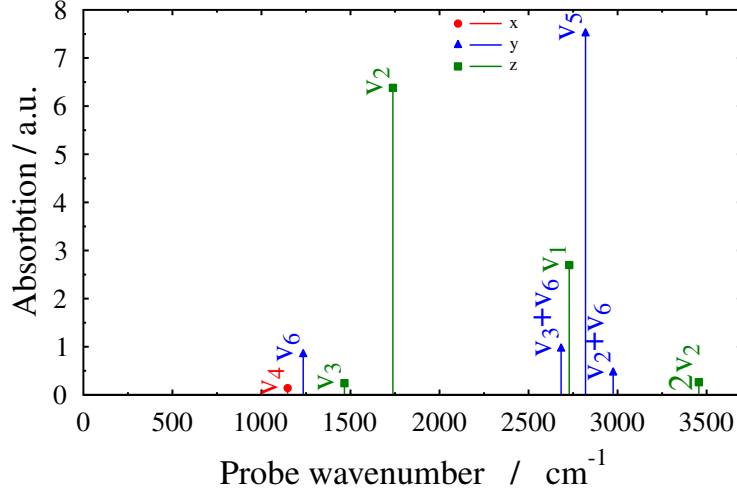


Figure 5: Field-free vibrational spectrum of the H_2CO molecule in its electronic ground state (X). The different peaks correspond to transitions from the vibrational ground state to vibrationally-excited eigenstates as indicated by the normal mode labels. Transitions polarized along the x , y and z axes are shown by the markers \bullet , \blacktriangle and \blacksquare , respectively.

where the numbers in the parentheses indicate the populations of the vibrational eigenstates in the initial field-dressed state. These data were then used to compute weighted field-dressed spectra, defined as the weighted average of field-free spectra whose initial states correspond to the X and A vibrational eigenstates that constitute the initial field-dressed state. Since the weights are chosen as the populations of the vibrational eigenstates in the initial field-dressed state, the weighted spectra are expected to be similar to the field-dressed spectra. Nevertheless, the absolute square of the transition amplitude expression in eqn (13) involves interference terms, therefore, the intensity patterns in the field-dressed spectra can differ from the ones in the weighted spectra. We note that as the dressing field is polarized along the body-fixed y axis and the body-fixed y component of the TDM transforms according to the B_1 irreducible representation, the X vibrational ground state (A_1 symmetry) can be coupled only to vibrational eigenstates of B_1 symmetry of the A electronic state by the dressing field. For all peaks shown in Fig. 6 the final field-dressed states remain eigenstates of the field-free molecule to a very good approximation and they can be written according to eqn (10) or eqn (11). Therefore, the considerations made below eqn (13) can be applied to decipher the field-dressed spectrum shown in Fig. 6.

A detailed analysis of the light-dressed spectrum in Fig. 6 has revealed that the peaks below 1100 cm^{-1} can be interpreted as transitions (both absorption and induced emission) from the vibrational eigenstates of A at 32931.2 cm^{-1} and 32937.2 cm^{-1} (both of B_1 symmetry) to other A vibrational eigenstates making up the final field-dressed states of eqn (11). The following qualitative conclusions have been drawn by investigating one-dimensional wave function cuts of the relevant A vibrational eigenstates: (a) the anharmonic nature of the V_A PES often leads to multiple changes in the vibrational quantum number v_4 ($|\Delta v_4| = 0, 1, 2, 3, \dots$), often accompanied by simultaneous changes in v_2 , v_3 and v_6 ; (b) the v_1 and v_5 modes hardly play any role; (c) the g_1 and g_2 transitions (x polarization) occur between A vibrational eigenstates of B_1 and A_1 symmetries (the x component of the PDM is of B_1 symmetry) and Δv_4 is always odd due to symmetry; (d) similarly, the g_3 (y polarization) and g_4 (z polarization) peaks involve transitions of $B_1 \rightarrow A_2$ and $B_1 \rightarrow B_1$ types, respectively, and Δv_4 is always even in both cases; (e) the emergence of peaks in the interval $0 - 1100\text{ cm}^{-1}$ can be understood as intensity borrowing according to the model introduced in Section 2.3. The intensity is borrowed from peaks that are also present in the field-free vibrational spectrum. In light of these conclusions, the richness of the field-dressed spectrum is primarily attributed to the v_4 mode. This statement is also corroborated by the field-free vibrational spectrum of H_2CO in its A electronic state, shown in Fig. 7. In Fig. 7 the initial state is chosen as the A vibrational ground state (GS) and therefore the field-

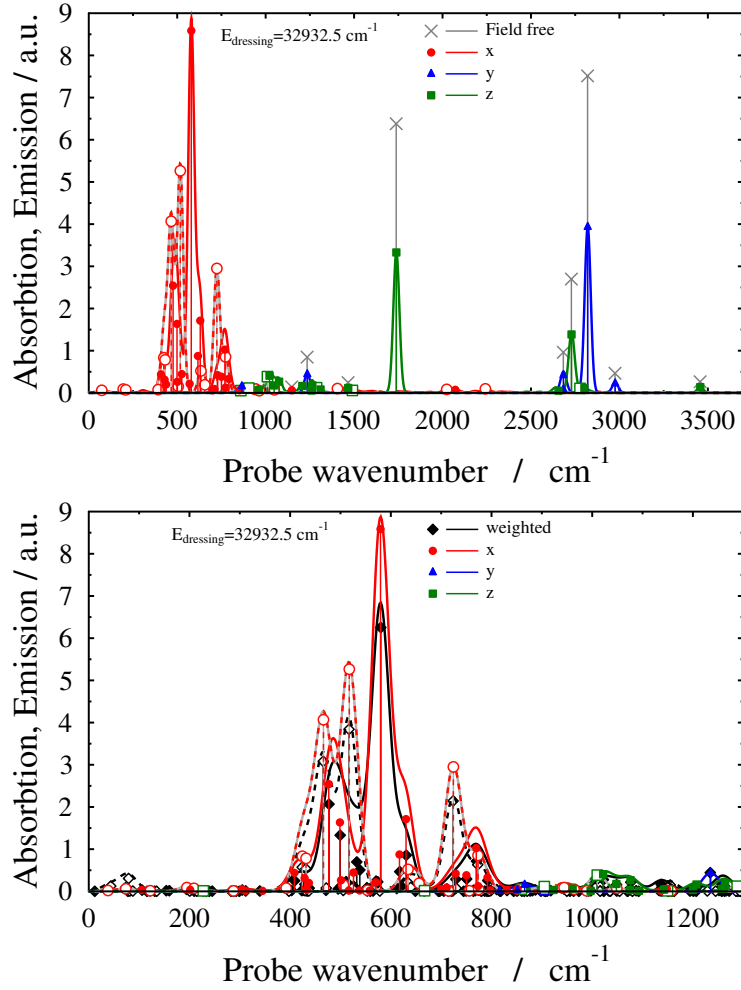


Figure 6: Absorption (solid line, full markers) and stimulated emission (dashed line, empty markers) spectra of H_2CO dressed with a laser field linearly polarized along the body-fixed y axis with $I_d = 10^{11} \text{ W/cm}^2$ and $\omega_d = 32932.5 \text{ cm}^{-1}$. Transitions polarized along the x , y and z axes are shown by the markers \bullet , \blacktriangle and \blacksquare , respectively. The field-dressed spectrum is compared to the field-free vibrational spectrum, denoted by the marker \times (upper panel). The weighted field-dressed spectrum (see text) is indicated by the marker \blacklozenge . The lower panel highlights the spectral range $0 - 1200 \text{ cm}^{-1}$, most relevant for the analysis of field-dressed spectra. Stick spectra were convolved with Gaussian functions having a full width at half maximum of 40 cm^{-1} . The most salient feature of the field-dressed spectrum, as opposed to the field-free vibrational spectrum, is the appearance of numerous peaks below 1100 cm^{-1} .

free vibrational spectrum in Fig. 7 is not directly relevant for our current analysis. It is apparent that, in contrast to the field-free vibrational spectrum of Fig. 5, the anharmonicity of the V_A PES along the ν_4 mode allows multiple changes in ν_4 , as justified by the appearance of the transitions $\text{GS} \rightarrow 2\nu_4$ and $\text{GS} \rightarrow 3\nu_4$ besides the fundamental transition $\text{GS} \rightarrow \nu_4$.

Two other interesting field-dressed spectra can be seen in Fig. 8 where the molecule is dressed with a laser field linearly polarized along the body-fixed y axis with $I_d = 10^{11} \text{ W/cm}^2$ and $\omega_d = 32935.0 \text{ cm}^{-1}$ ($\lambda_d = 303.63 \text{ nm}$) or $\omega_d = 32942.0 \text{ cm}^{-1}$ ($\lambda_d = 303.56 \text{ nm}$). Similarly to the field-dressed spectrum in Fig. 6, the g_1 , g_2 , g_3 and g_4 peaks all appear in the spectra of Fig. 8. In addition, another group of peaks is visible in the upper panel of Fig. 8, corresponding to x -polarized transitions below 100.0 cm^{-1} , involving $|\Delta\nu_4| = 1, 3$ and no change in the

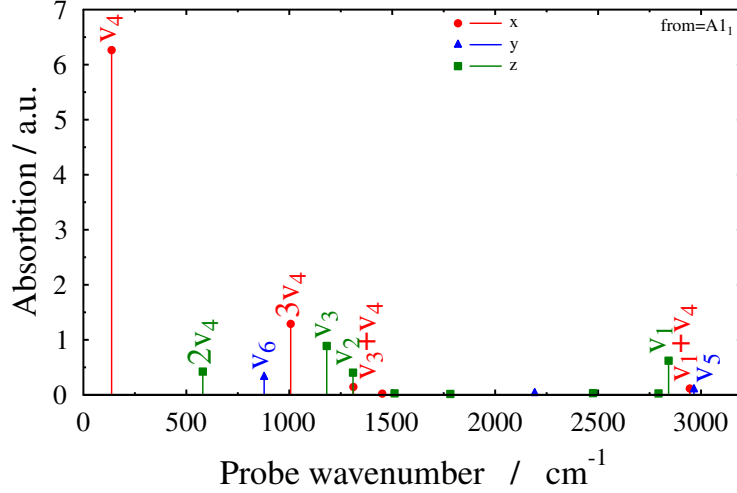


Figure 7: Field-free vibrational spectrum of the H_2CO molecule in its excited electronic state (A). The different peaks correspond to transitions from the vibrational ground state (GS) to vibrationally-excited eigenstates as indicated by the normal mode labels. Transitions polarized along the x , y and z axes are shown by the markers \bullet , \blacktriangle and \blacksquare , respectively. The appearance of the transitions $\text{GS} \rightarrow 2v_4$ and $\text{GS} \rightarrow 3v_4$ demonstrate the anharmonicity of the potential along the v_4 mode.

remaining vibrational modes. The composition of the initial field-dressed states for the field-dressed spectra shown in Fig. 8 helps identify the most relevant X and A vibrational eigenstates: X vibrational ground state (A_1 , 66.4%), A vibrational eigenstate of 32931.2 cm^{-1} (B_1 , 2.4%) and 32937.2 cm^{-1} (B_1 , 30.9%) ($\omega_d = 32935.0 \text{ cm}^{-1}$), and X vibrational ground state (A_1 , 43.0%), A vibrational eigenstate of 32937.2 cm^{-1} (B_1 , 9.3%) and 32943.2 cm^{-1} (B_1 , 47.6%) ($\omega_d = 32942.0 \text{ cm}^{-1}$). It is worth noting that Figs. 6 and 8 demonstrate how sensitive the field-dressed spectrum can be to small changes in ω_d . As the dressing field with the current ω_d values couples the X vibrational ground state to more close-lying A vibrational eigenstates (as shown in Fig. 3), small changes in ω_d , equivalent to slight shifts in the relative positions of the relevant X and A vibrational eigenstates, have a remarkable impact on the structure of the initial field-dressed state and thus on the intensity borrowing patterns in the field-dressed spectrum.

The considerations made so far in this section are further supported by the field-free vibrational spectra in Fig. 9 where the initial states have been chosen as the A vibrational eigenstates of 32931.2 cm^{-1} , 32937.2 cm^{-1} and 32943.2 cm^{-1} , having non-negligible populations in the previously described initial field-dressed states. As can be seen in Fig. 9, several transitions, originating from these eigenstates, appear below 1100 cm^{-1} in the field-free spectra. These transitions are strongly related to their field-dressed counterparts appearing in the field-dressed spectra shown in Figs. 6 and 8.

Switching to larger dressing wavenumbers ω_d , at certain values, similar remarkable intensity borrowing patterns appear in the lower part of the field-dressed spectrum. In Fig. 10, the three field-dressed spectra with dressing fields linearly polarized along the body-fixed y axis with $I_d = 10^{11} \text{ W/cm}^2$ and close-lying dressing wavenumbers of $\omega_d = 34189.5 \text{ cm}^{-1}$ ($\lambda_d = 292.49 \text{ nm}$), $\omega_d = 34193.0 \text{ cm}^{-1}$ ($\lambda_d = 292.46 \text{ nm}$) and $\omega_d = 34195.5 \text{ cm}^{-1}$ ($\lambda_d = 292.44 \text{ nm}$) clearly show the prominent features of intensity borrowing, which can again be interpreted by the considerations made earlier in this section.

Finally, one might notice that the dressing field has been polarized along the body-fixed y axis throughout our study, which was motivated by the strong first-order y -oriented TDM produced upon displacement along the v_4 vibrational mode. As the first derivatives of the x component of the TDM with respect to the coordinates are smaller than the corresponding values of the y TDM component and the first nonvanishing terms in the Taylor expansion of z component of the TDM are bilinear, effects induced by dressing fields polarized along the body-fixed y axis

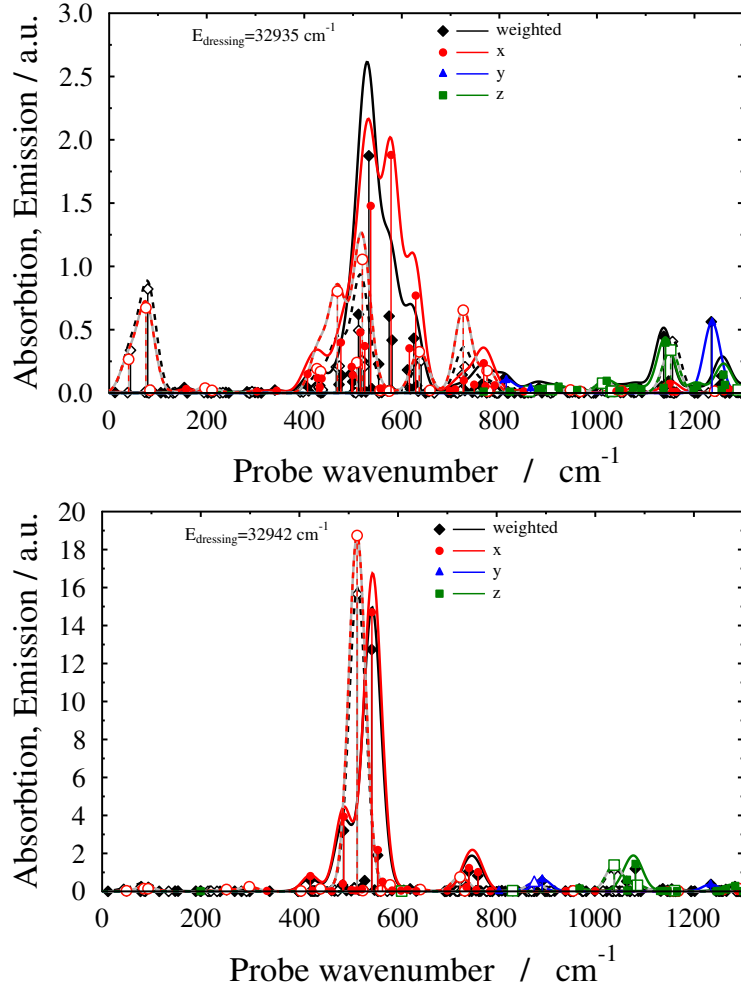


Figure 8: Absorption (solid line, full markers) and stimulated emission (dashed line, empty markers) spectra of H_2CO dressed with a laser field linearly polarized along the body-fixed y axis with $I_d = 10^{11} \text{ W/cm}^2$, $\omega_d = 32935.0 \text{ cm}^{-1}$ (upper panel) and $\omega_d = 32942.0 \text{ cm}^{-1}$ (lower panel). Transitions polarized along the x , y and z axes are shown by the markers \bullet , \blacktriangle and \blacksquare , respectively. The weighted field-dressed spectrum (see text) is indicated by the marker \blacklozenge . Stick spectra were convolved with Gaussian functions having a full width at half maximum of 40 cm^{-1} . The most salient features of the field-dressed spectrum, as opposed to the field-free vibrational spectrum, are the appearance of numerous peaks below 1100 cm^{-1} and the sensitivity of the spectrum to the frequency of the dressing laser.

are expected to be the most pronounced. The investigation of effects caused by the orientation of the dressing polarization vector in field-dressed spectra is left for future work.

4 Conclusions

In the present work we have outlined a pump-probe scheme to obtain the field-dressed low-energy vibronic spectra of polyatomic molecules treating all vibrational degrees of freedom. The H_2CO molecule which does not exhibit a natural conical intersection in the studied energy region was chosen as a showcase example. In order to calculate the weak-field absorption and stimulated emission spectra of the field-dressed H_2CO molecule we performed accurate,

six-dimensional computations for a multitude of dressing photon energies and dressing field intensities.

The results obtained clearly show the direct impact of the light-induced conical intersection on the field-dressed spectra of the H₂CO molecule. The findings are highly sensitive to variations of the dressing frequency which varies the location of the LICI, shedding light on the mixing of the levels of different electronic states and on their coupling mechanism. The emergence of peaks in the field-dressed spectrum below 1100 cm⁻¹ undoubtedly demonstrates strong nonadiabatic effects manifested in the so-called “intensity borrowing” phenomenon, arising due to the presence of the light-induced nonadiabaticity. The strong nonadiabaticity which is completely absent in the field-free H₂CO molecule mixes the different electronic and vibrational degrees of freedom creating a very rich pattern in a certain interval of the low-energy vibronic spectrum where no transitions occur in the field-free situation. This intense mixing process could not happen without the presence of the light-induced conical intersection.

Acknowledgements

Professor Joel Bowman is gratefully acknowledged for providing Fortran subroutines for the S₀ and S₁ potential energy surfaces. This research was supported by the EU-funded Hungarian grant EFOP-3.6.2-16-2017-00005. The authors are grateful to NKFIH for financial support (grants No. K128396 and PD124699).

References

- [1] H. Köppel, W. Domcke, and L. S. Cederbaum, *Multimode Molecular Dynamics Beyond the Born–Oppenheimer Approximation*, pp. 59–246. John Wiley & Sons, 2007.
- [2] D. R. Yarkony *Rev. Mod. Phys.*, vol. 68, pp. 985–1013, 1996.
- [3] M. Baer *Phys. Rep.*, vol. 358, no. 2, pp. 75 – 142, 2002.
- [4] G. A. Worth and L. S. Cederbaum *Ann. Rev. Phys. Chem.*, vol. 55, no. 1, pp. 127–158, 2004.
- [5] W. Domcke, D. R. Yarkony, and H. Köppel, *Conical Intersections*. World Scientific, 2004.
- [6] M. Baer, *Beyond Born Oppenheimer: Electronic Non-Adiabatic Coupling Terms and Conical Intersections*. Wiley, New York, 2006.
- [7] J. S. Lim and S. K. Kim *Nat. Chem.*, vol. 2, no. 8, pp. 627–632, 2010.
- [8] D. Polli, P. Altoè, O. Weingart, K. M. Spillane, C. Manzoni, D. Brida, G. Tomasello, G. Orlandi, P. Kukura, R. A. Mathies, M. Garavelli, and G. Cerullo *Nature*, vol. 467, no. 7314, pp. 440–443, 2010.
- [9] H. J. Wörner, J. B. Bertrand, B. Fabre, J. Higuët, H. Ruf, A. Dubrouil, S. Patchkovskii, M. Spanner, Y. Mairesse, V. Blanchet, E. Mével, E. Constant, P. B. Corkum, and D. M. Villeneuve *Science*, vol. 334, no. 6053, pp. 208–212, 2011.
- [10] H. S. You, S. Han, J. S. Lim, and S. K. Kim *J. Phys. Chem. Lett.*, vol. 6, no. 16, pp. 3202–3208, 2015.
- [11] A. J. Musser, M. Liebel, C. Schnedermann, T. Wende, T. B. Kehoe, A. Rao, and P. Kukura *Nat. Phys.*, vol. 11, no. 4, pp. 352–357, 2015.
- [12] A. von Conta, A. Tehlar, A. Schletter, Y. Arasaki, K. Takatsuka, and H. J. Wörner *Nat. Commun.*, vol. 9, no. 1, p. 3162, 2018.
- [13] M. E. Corrales, J. González-Vázquez, R. de Nalda, and L. Bañares *J. Phys. Chem. Lett.*, vol. 10, no. 2, pp. 138–143, 2019.

- [14] M. N. R. Ashfold, A. L. Devine, R. N. Dixon, G. A. King, M. G. D. Nix, and T. A. A. Oliver *Proc. Natl. Acad. Sci. U.S.A.*, vol. 105, no. 35, pp. 12701–12706, 2008.
- [15] T. J. Martinez *Nature*, vol. 467, no. 7314, pp. 412–413, 2010.
- [16] B. F. E. Curchod and T. J. Martínez *Chem. Rev.*, vol. 118, no. 7, pp. 3305–3336, 2018.
- [17] M. Kowalewski, K. Bennett, K. E. Dorfman, and S. Mukamel *Phys. Rev. Lett.*, vol. 115, p. 193003, 2015.
- [18] K. Bennett, M. Kowalewski, J. R. Rouxel, and S. Mukamel *Proc. Natl. Acad. Sci. U.S.A.*, vol. 115, no. 26, pp. 6538–6547, 2018.
- [19] M. Born and R. Oppenheimer *Ann. Phys.*, vol. 389, no. 20, pp. 457–484, 1927.
- [20] J. von Neumann and E. P. Wigner *Z. Physik*, vol. 30, pp. 467–470, 1929.
- [21] N. Moiseyev, M. Šindelka, and L. S. Cederbaum *J. Phys. B: At. Mol. Opt. Phys.*, vol. 41, p. 221001, 2008.
- [22] M. Šindelka, N. Moiseyev, and L. S. Cederbaum *J. Phys. B: At. Mol. Opt. Phys.*, vol. 44, p. 045603, 2011.
- [23] G. J. Halász, Á. Vibók, M. Šindelka, N. Moiseyev, and L. S. Cederbaum *J. Phys. B: At. Mol. Opt. Phys.*, vol. 44, p. 175102, 2011.
- [24] G. J. Halász, M. Šindelka, N. Moiseyev, L. S. Cederbaum, and A. Vibók *J. Phys. Chem. A*, vol. 116, no. 11, pp. 2636–2643, 2012.
- [25] G. J. Halász, A. Vibók, N. Moiseyev, and L. S. Cederbaum *Phys. Rev. A*, vol. 88, p. 043413, 2013.
- [26] G. J. Halász, P. Badankó, and A. Vibók *Mol. Phys.*, vol. 116, no. 19-20, pp. 2652–2659, 2018.
- [27] A. Natan, M. R. Ware, V. S. Prabhudesai, U. Lev, B. D. Bruner, O. Heber, and P. H. Bucksbaum *Phys. Rev. Lett.*, vol. 116, p. 143004, 2016.
- [28] G. J. Halász, A. Vibók, and L. S. Cederbaum *J. Phys. Chem. Lett.*, vol. 6, no. 3, pp. 348–354, 2015.
- [29] A. Csehi, G. J. Halász, L. S. Cederbaum, and A. Vibók *Faraday Discuss.*, vol. 194, pp. 479–493, 2016.
- [30] A. Csehi, G. J. Halász, L. S. Cederbaum, and A. Vibók *Phys. Chem. Chem. Phys.*, vol. 19, pp. 19656–19664, 2017.
- [31] A. Csehi, G. J. Halász, L. S. Cederbaum, and A. Vibók, “Chapter 6 light-induced conical intersections,” in *Attosecond Molecular Dynamics*, pp. 183–217, The Royal Society of Chemistry, 2018.
- [32] T. Szidarovszky, G. J. Halász, A. G. Császár, L. S. Cederbaum, and A. Vibók *J. Phys. Chem. Lett.*, vol. 9, no. 11, pp. 2739–2745, 2018.
- [33] T. Szidarovszky, G. J. Halász, A. G. Császár, L. S. Cederbaum, and A. Vibók *J. Phys. Chem. Lett.*, vol. 9, no. 21, pp. 6215–6223, 2018.
- [34] T. Szidarovszky, A. G. Császár, G. J. Halász, and A. Vibók *Phys. Rev. A*, vol. 100, p. 033414, 2019.
- [35] M. Pawlak, T. Szidarovszky, G. J. Halász, and A. Vibók *Phys. Chem. Chem. Phys.*, vol. 22, pp. 3715–3723, 2020.
- [36] J. Kim, H. Tao, J. L. White, V. S. Petrović, T. J. Martinez, and P. H. Bucksbaum *J. Phys. Chem. A*, vol. 116, no. 11, pp. 2758–2763, 2012.

- [37] M. E. Corrales, J. González-Vázquez, G. Balerdi, I. R. Solá, R. de Nalda, and L. Bañares *Nat. Chem.*, vol. 6, no. 9, pp. 785–790, 2014.
- [38] P. V. Demekhin and L. S. Cederbaum *J. Chem. Phys.*, vol. 139, no. 15, p. 154314, 2013.
- [39] M. Araujo, B. Lasorne, M. J. Bearpark, and M. A. Robb *J. Phys. Chem. A*, vol. 112, no. 33, pp. 7489–7491, 2008.
- [40] M. Araújo, B. Lasorne, A. L. Magalhães, G. A. Worth, M. J. Bearpark, and M. A. Robb *J. Chem. Phys.*, vol. 131, no. 14, p. 144301, 2009.
- [41] M. Araújo, B. Lasorne, A. L. Magalhães, M. J. Bearpark, and M. A. Robb *J. Phys. Chem. A*, vol. 114, no. 45, pp. 12016–12020, 2010.
- [42] S. Chu *J. Chem. Phys.*, vol. 75, no. 5, pp. 2215–2221, 1981.
- [43] S.-I. Chu and D. A. Telnov *Phys. Rep.*, vol. 390, no. 1, pp. 1 – 131, 2004.
- [44] E. Mátyus, G. Czakó, and A. G. Császár *J. Chem. Phys.*, vol. 130, no. 13, p. 134112, 2009.
- [45] C. Fábri, E. Mátyus, and A. G. Császár *J. Chem. Phys.*, vol. 134, no. 7, p. 074105, 2011.
- [46] A. Tóth, A. Csehi, G. J. Halász, and A. Vibók *Phys. Rev. A*, vol. 99, p. 043424, 2019.
- [47] P. Bunker and P. Jensen, *Molecular Symmetry and Spectroscopy*. NRC Research Press, 2006.
- [48] X. Wang, P. L. Houston, and J. M. Bowman *Philos. Trans. R. Soc. A*, vol. 375, no. 2092, p. 20160194, 2017.
- [49] B. Fu, B. C. Shepler, and J. M. Bowman *J. Am. Chem. Soc.*, vol. 133, no. 20, pp. 7957–7968, 2011.
- [50] R. S. Mulliken *J. Chem. Phys.*, vol. 23, no. 11, pp. 1997–2011, 1955.
- [51] A. G. Császár, C. Fábri, T. Szidarovszky, E. Mátyus, T. Furtenbacher, and G. Czakó *Phys. Chem. Chem. Phys.*, vol. 14, pp. 1085–1106, 2012.
- [52] X. Chapuisat and C. Iung *Phys. Rev. A*, vol. 45, pp. 6217–6235, 1992.
- [53] C. Eckart *Phys. Rev.*, vol. 47, pp. 552–558, 1935.
- [54] E. Mátyus, G. Czakó, B. T. Sutcliffe, and A. G. Császár *J. Chem. Phys.*, vol. 127, no. 8, p. 084102, 2007.
- [55] C. Fábri, E. Mátyus, T. Furtenbacher, L. Nemes, B. Mihály, T. Zoltáni, and A. G. Császár *J. Chem. Phys.*, vol. 135, no. 9, p. 094307, 2011.
- [56] M. J. Frisch, G. W. Trucks, H. B. Schlegel, G. E. Scuseria, M. A. Robb, J. R. Cheeseman, G. Scalmani, V. Barone, B. Mennucci, G. A. Petersson, H. Nakatsuji, M. Caricato, X. Li, H. P. Hratchian, A. F. Izmaylov, J. Bloino, G. Zheng, J. L. Sonnenberg, M. Hada, M. Ehara, K. Toyota, R. Fukuda, J. Hasegawa, M. Ishida, T. Nakajima, Y. Honda, O. Kitao, H. Nakai, T. Vreven, J. A. Montgomery, Jr., J. E. Peralta, F. Ogliaro, M. Bearpark, J. J. Heyd, E. Brothers, K. N. Kudin, V. N. Staroverov, R. Kobayashi, J. Normand, K. Raghavachari, A. Rendell, J. C. Burant, S. S. Iyengar, J. Tomasi, M. Cossi, N. Rega, J. M. Millam, M. Klene, J. E. Knox, J. B. Cross, V. Bakken, C. Adamo, J. Jaramillo, R. Gomperts, R. E. Stratmann, O. Yazyev, A. J. Austin, R. Cammi, C. Pomelli, J. W. Ochterski, R. L. Martin, K. Morokuma, V. G. Zakrzewski, G. A. Voth, P. Salvador, J. J. Dannenberg, S. Dapprich, A. D. Daniels, O. Farkas, J. B. Foresman, J. V. Ortiz, J. Cioslowski, and D. J. Fox, “Gaussian 09 Revision D.01.” Gaussian Inc. Wallingford CT 2009.

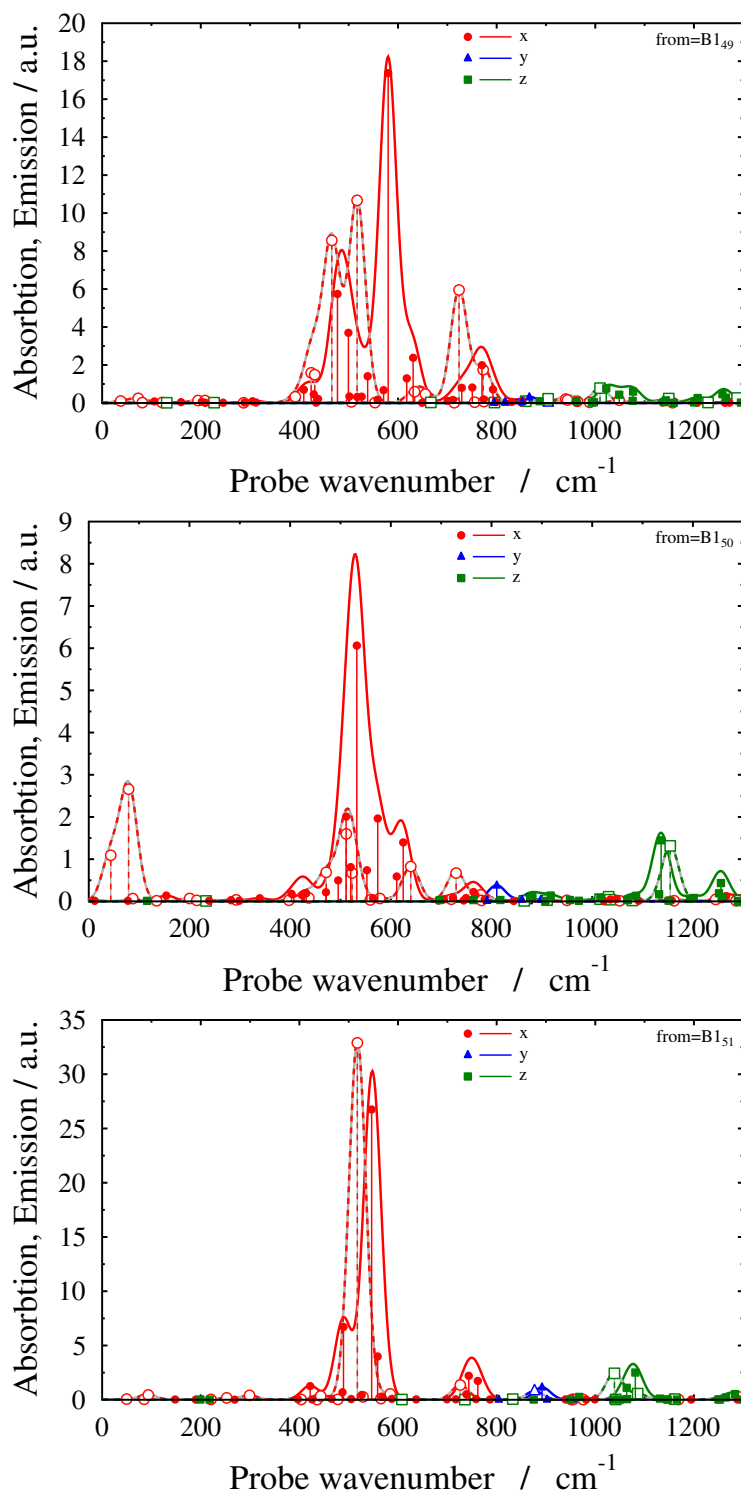


Figure 9: Field-free vibrational spectra (absorption: solid line with full markers, stimulated emission: dashed line with empty markers) of the H_2CO molecule in its excited electronic state (A). The different peaks correspond to transitions from an excited vibrational eigenstate (32931.2 cm^{-1} : upper panel, 32937.2 cm^{-1} : middle panel, 32943.2 cm^{-1} : lower panel) to other vibrational eigenstates. Transitions polarized along the x , y and z axes are shown by the markers \bullet , \blacktriangle and \blacksquare , respectively. Stick spectra were convolved with Gaussian functions having a full width at half maximum of 40 cm^{-1} .

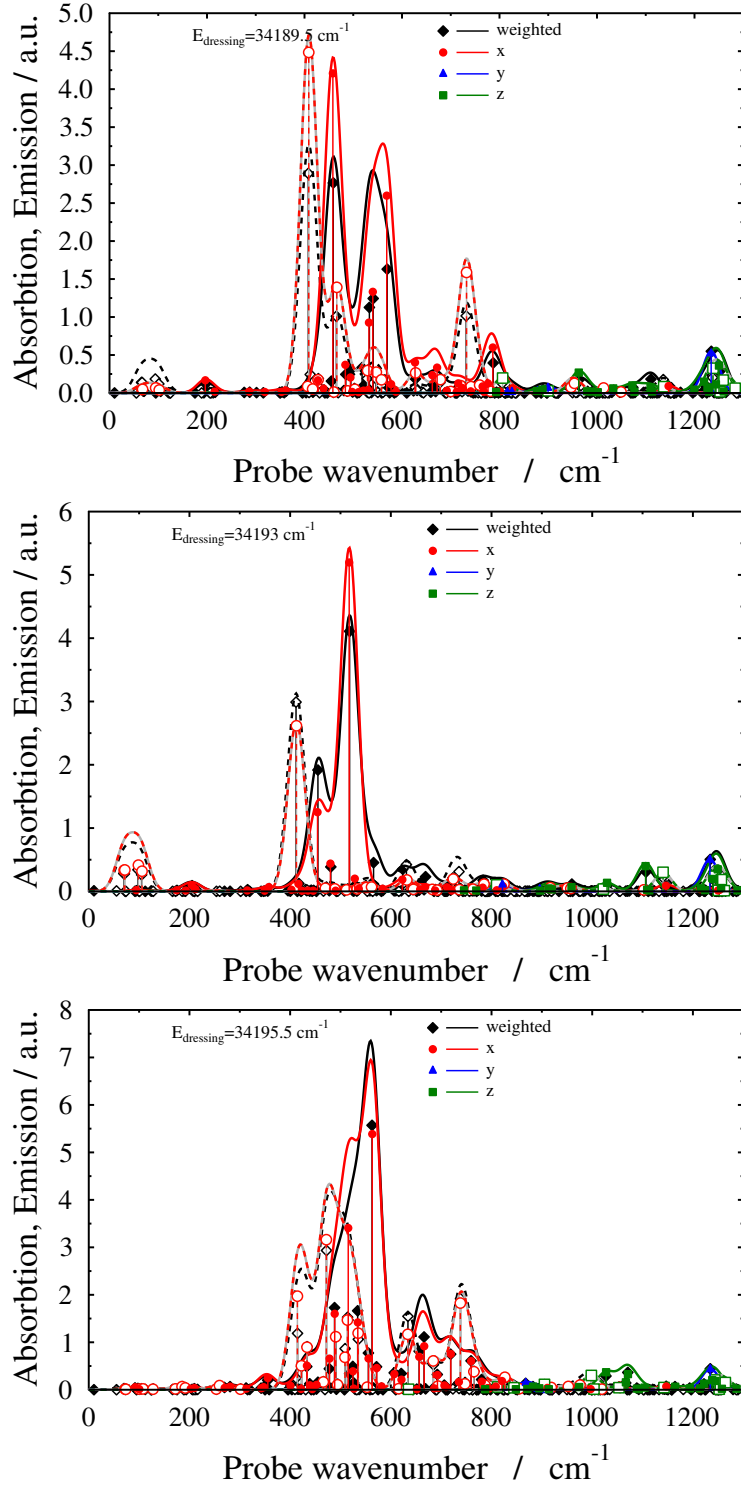


Figure 10: Absorption (solid line, full markers) and stimulated emission (dashed line, empty markers) spectra of H_2CO dressed with a laser field linearly polarized along the body-fixed y axis with $I_d = 10^{11} \text{ W/cm}^2$, $\omega_d = 34189.5 \text{ cm}^{-1}$ (upper panel), $\omega_d = 34193.0 \text{ cm}^{-1}$ (middle panel) and $\omega_d = 34195.5 \text{ cm}^{-1}$ (lower panel). Transitions polarized along the x , y and z axes are shown by the markers \bullet , \blacktriangle and \blacksquare , respectively. The weighted field-dressed spectrum (see text) is indicated by the marker \blacklozenge . Stick spectra were convolved with Gaussian functions having a full width at half maximum of 40 cm^{-1} . The most salient feature of the field-dressed spectrum, as opposed to the field-free vibrational spectrum, are the appearance of numerous peaks below 1100 cm^{-1} and the sensitivity of the spectrum to the frequency of the dressing laser.